Iranian Journal of Astronomy and Astrophysics
Vol. 12, No. 4, Autumn 2025, 311–322
©Available online at http://ijaa.du.ac.ir
DOI: 10.22128/ijaa.2026.3224.1243
Online ISSN: 2383–403X

Iranian Journal of Astronomy and Astrophysics

Research Paper

Evolutionary Structure of Magnetized Accretion Flow Incorporating Saturated Thermal Conduction

Kazem Faghei*[1] · Motahareh Mohammadpour[2]

[1] School of Physics, Damghan University, Damghan, Iran;
*E-mail: kfaghei@du.ac.ir

[2] School of Physics, Damghan University, Damghan, Iran;
E-mail: mohammadpour@du.ac.ir

Received: 26 January 2026; **Accepted:** 26 February 2026; **Published:** 14 March 2026

Abstract. This paper presents a time-dependent model for magnetized, advection-dominated accretion flows (ADAFs) that incorporates non-ideal effects, specifically resistivity and saturated thermal conduction. We apply a self-similar method to transform the full time-dependent magnetohydrodynamic (MHD) equations into a set of coupled ordinary differential equations, enabling us to investigate the evolving radial structure influenced by turbulent viscosity, magnetic diffusivity, and non-local energy transport. The resulting solutions confirm that the flow structure is inherently time-dependent. Numerical results demonstrate that increasing the efficiency of outward energy transport via saturated conduction weakens turbulence, reduces dissipation and temperature, increases density, and reduces the radial infall velocity while increasing the rotational velocity. In contrast, stronger magnetization leads to enhanced magnetic fields, lower temperatures, and faster radial inflow. We further show that the turbulence prescription parameter, which controls the pressure dependence of transport coefficients, significantly influences the balance between magnetic and thermal support. This framework offers a dynamic perspective on magnetized accretion flows, highlighting how non-ideal magnetic effects and conduction regulate the flow structure.

Keywords: Accretion, Accretion Discs, Conduction, Magnetohydrodynamics: MHD.

1 Introduction

Accretion flows onto compact objects such as black holes and neutron stars exist in various regimes, with hot, geometrically thick, and advection-dominated accretion flows (ADAFs) describing systems with low mass accretion rates [1,2]. In these hot, optically thin plasmas, the traditional assumption of local radiative energy balance breaks down, and a significant fraction of the dissipated gravitational energy is advected inward rather than radiated away. Thermal conduction plays a particularly important role in such environments due to the high temperature and low density, which lead to a long electron mean free path and place conduction in the saturated regime [3]. This non-local energy transport can substantially modify the thermal structure and stability of the flow by redistributing heat radially, as noted in studies of hot accretion flows [4]. High-resolution magnetohydrodynamic (MHD) simulations of hot accretion flows including thermal conduction have demonstrated that conduction

* *Corresponding author*

plays an important role in redistributing thermal energy and shaping the temperature and wind structure of the flow [5].

Magnetic fields are essential components of accretion dynamics, contributing to angular momentum transport via MHD turbulence and potentially driving outflows. In differentially rotating flows, radial field components are wound up to produce toroidal fields [6,7]. This toroidal component contributes both magnetic pressure and tension forces that can significantly influence the flow's structure, stability, and dynamical evolution [8]. Moreover, in the hot, low-density ADAF regime, magnetic pressure can become comparable to gas pressure, necessitating self-consistent treatment of magnetic support. Beyond ideal MHD, resistive effects become important in weakly ionized or turbulent plasmas, enabling Ohmic dissipation [9,10]. Recent studies have shown that including magnetic diffusivity can significantly alter the thermal and dynamical properties of accretion flows [11].

Significant insight into the behavior of such complex systems has been gained through semi-analytical self-similar solutions, which reveal scaling relationships and parameter dependencies. Faghei (2012) developed a steady-state, self-similar model for viscous and resistive ADAFs that incorporated both magnetic diffusivity and saturated thermal conduction [10]. This work demonstrated how resistivity and conduction jointly affect the structure and energy balance of magnetized accretion flows. However, the steady-state formulation precludes investigation of temporal evolution, which is crucial for understanding flow responses to instabilities, variable boundary conditions, or transient phenomena often observed in accreting systems [12].

In this paper, we extend the framework of Faghei (2012) by constructing a *time-dependent* model for magnetized, advection-dominated accretion flows with both resistivity and saturated thermal conduction [10]. We derive a set of self-similar ordinary differential equations from the full time-dependent partial differential equations, enabling us to investigate how magnetic tension, turbulent viscosity and diffusivity, advection, and non-local thermal conduction collectively shape the evolving radial structure of the flow. Our model provides boundary conditions for numerical integration and offers a more dynamic perspective on hot accretion than previously available in semi-analytical resistive MHD studies.

2 Basic Equations

We investigate the dynamical behavior of a hot, magnetized accretion flow by constructing a simplified model in spherical coordinates (r, θ, ϕ) centered on a central object of mass M_*. We consider the flow in the equatorial plane ($\theta = \pi/2$), assuming axisymmetry ($\partial/\partial\phi = 0$) and neglecting all latitudinal dependencies, so that all physical quantities depend only on the radial coordinate r and time t. Self-gravity of the accreting gas and general relativistic corrections are neglected. Therefore, the gravitational potential of the central mass is described by the Newtonian form $\Phi = -GM_*/r$. The model incorporates a toroidal magnetic field B_φ and extends previous work by self-consistently including the effects of both saturated thermal conduction and resistivity, allowing for a more realistic treatment that includes non-ideal MHD effects. Under the above assumptions, the dynamics of the accretion flow are governed by the following set of equations.

The conservation of mass is expressed by the continuity equation

$$\frac{\partial \rho}{\partial t} + \frac{1}{r^2}\frac{\partial}{\partial r}\left(r^2 \rho v_r\right) = 0, \tag{1}$$

where ρ is the mass density and v_r is the radial velocity.

The radial momentum conservation is given by

$$\frac{\partial v_r}{\partial t} + v_r \frac{\partial v_r}{\partial r} + \frac{1}{\rho}\frac{\partial p_g}{\partial r} + \frac{GM_*}{r^2} - r\Omega^2 + \frac{1}{4\pi\rho}\frac{B_\varphi}{r}\frac{\partial}{\partial r}\left(rB_\varphi\right) = 0, \tag{2}$$

where p_g is the gas pressure, Ω is the angular velocity, and the last term represents the magnetic tension force associated with the toroidal magnetic field.

Angular momentum transport satisfies

$$\rho\left[\frac{\partial}{\partial t}\left(r^2\Omega\right) + v_r\frac{\partial}{\partial r}\left(r^2\Omega\right)\right] = \frac{1}{r^2}\frac{\partial}{\partial r}\left(\nu\rho r^4\frac{\partial\Omega}{\partial r}\right), \tag{3}$$

where ν is the kinematic viscosity coefficient.

The evolution of the toroidal magnetic field follows from the induction equation, including magnetic diffusivity

$$\frac{\partial B_\varphi}{\partial t} + \frac{1}{r}\frac{\partial}{\partial r}\left[rv_rB_\varphi - \eta\frac{\partial}{\partial r}\left(rB_\varphi\right)\right] = 0, \tag{4}$$

where η denotes the magnetic diffusivity.

Here, we assume that both ν and η arise from turbulent processes within the accretion flow [9] and references therein. We therefore adopt a generalized parameterization expressing these coefficients as

$$\nu = \alpha\frac{p_g}{\rho\Omega_K}(1+\mu)^{1-n}, \tag{5}$$

$$\eta = \eta_0\frac{p_g}{\rho\Omega_K}(1+\mu)^{1-n}, \tag{6}$$

where α and η_0 are dimensionless parameters characterizing the efficiency of turbulent viscosity and magnetic diffusivity, respectively; $\Omega_K = \sqrt{GM_*/r^3}$ is the Keplerian angular velocity; and μ is the disk magnetization defined as the ratio of magnetic to gas pressure,

$$\mu = \frac{B_\varphi^2/8\pi}{p_g}. \tag{7}$$

The exponent n is a free parameter that switches between different turbulence prescriptions, e.g., $n = 0$ corresponds to total pressure support, while $n = 1$ corresponds to gas pressure support. This formulation implies a constant magnetic Prandtl number,

$$Pm = \frac{\nu}{\eta} = \frac{\alpha}{\eta_0}, \tag{8}$$

which is a common assumption in semi-analytical models of turbulent accretion disks. The dependence on $(1+\mu)$ introduces a feedback mechanism whereby the magnetic field strength directly influences the efficiencies of angular momentum transport and magnetic diffusion.

The energy equation governing the accretion flow can be written as

$$\frac{1}{\gamma-1}\left(\frac{\partial p_g}{\partial t} + v_r\frac{\partial p_g}{\partial r}\right) + \frac{\gamma}{\gamma-1}\frac{p_g}{r^2}\frac{\partial}{\partial r}\left(r^2v_r\right) = Q_{\rm vis} + Q_{\rm res} - Q_{\rm rad} - Q_{\rm cond}, \tag{9}$$

where γ is the adiabatic index. The terms on the right-hand side correspond to various heating and cooling processes, defined as follows. The viscous heating rate per unit volume is

$$Q_{\rm vis} = \nu\rho r^2\left(\frac{\partial\Omega}{\partial r}\right)^2, \tag{10}$$

and the resistive heating rate due to magnetic diffusivity is

$$Q_{\rm res} = \frac{\eta}{4\pi r^2}\left[\frac{\partial}{\partial r}(rB_\varphi)\right]^2. \tag{11}$$

Thermal conduction contributes an energy transport term of the form

$$Q_{\rm cond} = \frac{1}{r^2}\frac{\partial}{\partial r}\left(r^2 F_{\rm sat}\right). \tag{12}$$

Because of the plasma is low density and high temperature, the electron mean free path is large and conduction operates in the saturated regime [3]. The saturated conductive flux is given by

$$F_{\rm sat} = 5\phi_s p_g \left(\frac{p_g}{\rho}\right)^{1/2} = 5\phi_s \rho c_s^3, \tag{13}$$

where $c_s = \sqrt{p_g/\rho}$ is the isothermal sound speed, and ϕ_s is a dimensionless saturation constant of order unity. The flow is assumed to be radiatively inefficient. We characterize this by defining the advection factor f as the fraction of the total heating that is advected inward rather than radiated away. Accordingly, the radiative cooling term is written as

$$Q_{\rm rad} = (1-f)\left(Q_{\rm vis} + Q_{\rm res}\right), \tag{14}$$

with $0 \le f \le 1$; here, $f = 1$ corresponds to full advection dominance with negligible radiation losses. This energy balance accounts for viscous and resistive heating, radiative cooling, and non-local energy transport by saturated thermal conduction, providing a comprehensive thermodynamic description of the magnetized accretion flow. The advective transport of energy can be written by substituting equations (10)–(12), and (14) into equation (9) as

$$\begin{aligned} Q_{\rm adv} &= \frac{1}{\gamma-1}\left(\frac{\partial p_g}{\partial t} + v_r\frac{\partial p_g}{\partial r}\right) + \frac{\gamma}{\gamma-1}\frac{p_g}{r^2}\frac{\partial}{\partial r}\left(r^2 v_r\right) \\ &= f\left\{\nu\rho r^2\left(\frac{\partial\Omega}{\partial r}\right)^2 + \frac{\eta}{4\pi r^2}\left[\frac{\partial}{\partial r}(rB_\varphi)\right]^2\right\} - \frac{1}{r^2}\frac{\partial}{\partial r}\left(r^2 F_{\rm sat}\right). \end{aligned}$$

This set of equations (1)–(4), and (15) defines our time-dependent model for a resistive, advection-dominated magnetized accretion flow with saturated thermal conduction.

3 Self-similar solutions

To obtain time-dependent solutions of the governing equations, we employ a self-similar transformation inspired by the natural scaling of the problem. We define the similarity variable ξ and express physical variables in terms of ξ and time t as follows

$$r = (GM_*)^{1/3}\,\xi\, t^{2/3}, \tag{15}$$

$$\rho(r,t) = \left(\frac{\dot M_0}{GM_*}\right) R(\xi)\, t^{-1}, \tag{16}$$

$$p_g(r,t) = \left(\frac{\dot M_0^3}{GM_*}\right)^{1/3} P(\xi)\, t^{-5/3}, \tag{17}$$

$$v_r(r,t) = (GM_*)^{1/3} V(\xi)\, t^{-1/3}, \tag{18}$$

$$\Omega(r,t) = W(\xi)\, t^{-1}, \tag{19}$$

$$B_\varphi(r,t) = \left(\frac{\dot{M}_0^3}{GM_*}\right)^{1/6} B(\xi)\, t^{-5/6}, \tag{20}$$

where $\dot{M}_0$ is a constant mass accretion rate scale, chosen to represent the characteristic mass inflow of the system, and $R(\xi)$, $P(\xi)$, $V(\xi)$, $W(\xi)$, and $B(\xi)$ are dimensionless functions of the similarity coordinate ξ.

The mass accretion rate is self-similarly scaled as

$$\dot{M}(r,t) = \dot{M}_0 \dot{m}(\xi). \tag{21}$$

Substituting these transformations into the basic system of equations (1)–(4), and the energy equation (15), reduces the partial differential equations (PDEs) to a set of coupled ordinary differential equations (ODEs) in ξ

$$\left(V - \frac{2\xi}{3}\right)\frac{dR}{d\xi} - R + \frac{R}{\xi^2}\frac{d}{d\xi}\left(\xi^2 V\right) = 0, \tag{22}$$

$$\left(V - \frac{2\xi}{3}\right)\frac{dV}{d\xi} - \frac{V}{3} + \frac{1}{R}\frac{dP}{d\xi} - \xi\left(W^2 - \xi^{-3}\right) + \frac{B}{4\pi\xi R}\frac{d}{d\xi}\left(\xi B\right) = 0, \tag{23}$$

$$R\left[\left(V - \frac{2\xi}{3}\right)\frac{d}{d\xi}(\xi^2 W) + \frac{1}{3}\xi^2 W\right] = \frac{\alpha}{\xi^2}\frac{d}{d\xi}\left[\left(1 + \frac{B^2}{8\pi P}\right)^{1-n} P\xi^{\frac{11}{2}}\frac{dW}{d\xi}\right], \tag{24}$$

$$\frac{1}{\gamma - 1}\left[\left(V - \frac{2\xi}{3}\right)\frac{dP}{d\xi} - \frac{5P}{3}\right] + \frac{\gamma}{\gamma - 1}\frac{P}{\xi^2}\frac{d}{d\xi}(\xi^2 V) =$$
$$fP\left(1 + \frac{B^2}{8\pi P}\right)^{1-n}\left[\alpha\xi^{\frac{7}{2}}\left(\frac{dW}{d\xi}\right)^2 + \frac{\eta_0}{4\pi R}\xi^{-\frac{1}{2}}\left(\frac{d}{d\xi}(\xi B)\right)^2\right] - \frac{5\phi_s}{\xi^2}\frac{d}{d\xi}\left(\xi^2 P\sqrt{\frac{P}{R}}\right), \tag{25}$$

$$\left(V - \frac{2\xi}{3}\right)\frac{dB}{d\xi} - \frac{5B}{6} + \frac{B}{\xi}\frac{d}{d\xi}(\xi V) - \frac{\eta_0}{\xi}\frac{d}{d\xi}\left[\frac{P}{R}\xi^{\frac{3}{2}}\left(1 + \frac{B^2}{8\pi P}\right)^{1-n}\frac{d}{d\xi}(\xi B)\right] = 0. \tag{26}$$

These equations govern the radial profiles of density, pressure, velocity, angular velocity, and magnetic field strength, encapsulating the effects of magnetic diffusivity, viscosity, saturated conduction, and advection.

3.1 Asymptotic solutions near the center

To understand the behavior of the flow near the central object ($\xi \to 0$), we seek asymptotic power-law solutions for the dimensionless variables. We express these as expansions of the form

$$R(\xi) \sim \xi^{-3/2}\left(R_0 + R_1\xi + \cdots\right), \tag{27}$$

$$P(\xi) \sim \xi^{-5/2}\left(P_0 + P_1\xi + \cdots\right), \tag{28}$$

$$V(\xi) \sim \xi^{-1/2}\left(V_0 + V_1\xi + \cdots\right), \tag{29}$$

$$W(\xi) \sim \xi^{-3/2}\left(W_0 + W_1\xi + \cdots\right), \tag{30}$$

$$B(\xi) \sim \xi^{-5/4}\left(B_0 + B_1\xi + \cdots\right). \tag{31}$$

Substituting these expansions into the system of ordinary differential equations (22)–(26) and collecting terms at the leading order yields a set of algebraic relations between the coefficients $\{R_0, P_0, V_0, W_0, B_0\}$.

In particular, the coefficient R_0 satisfies an implicit nonlinear equation given by

$$\left\{ f(\gamma-1)\left[\frac{(864\pi^2 R_0^2 - 27\dot{m}_{\rm in}^2)\alpha^2(1+\mu)^{(1-n)}}{6\pi R_0 \alpha} + \frac{8\big((-9\mu-45)\alpha+\mu\eta_0\big)\dot{m}_{\rm in}R_0\pi}{6\pi R_0\alpha} \right] + 24\dot{m}_{\rm in}(\gamma-5/3) \right\} \times \sqrt{\frac{6\dot{m}_{\rm in}}{\pi(1+\mu)^{(1-n)}\alpha R_0}} - \frac{320\phi_s \dot{m}_{\rm in}(\gamma-1)}{(1+\mu)^{(1-n)}\alpha} = 0 \tag{32}$$

The other coefficients can be expressed approximately as

$$P_0 \approx \frac{\dot{m}_{\rm in}}{6\pi(1+\mu_{\rm in})^{1-n}\alpha}, \tag{33}$$

$$V_0 \approx -\frac{\dot{m}_{\rm in}}{4\pi R_0}, \tag{34}$$

$$W_0 = \sqrt{\frac{\alpha\,(R_0^2\pi^2 - \dot{m}_{\rm in}^2/32)\,(1+\mu_{\rm in})^{1-n} - \dot{m}_{\rm in}R_0\pi(\mu_{\rm in}+5)/12}{R_0^2\pi^2\alpha(1+\mu_{\rm in})^{n-1}}} \tag{35}$$

$$B_0 \approx \sqrt{\frac{4\,\dot{m}_{\rm in}\,\mu_{in}}{3(1+\mu_{\rm in})^{1-n}\alpha}}. \tag{36}$$

Here, $\dot{m}_{\rm in}$ and $\mu_{\rm in}$ denote respectively the dimensionless mass accretion rate and the magnetization parameter near the inner boundary $\xi_{\rm in}$. These parameters are defined in terms of the leading coefficients as

$$\dot{m}_{\rm in} \approx -4\pi R_0 V_0, \tag{37}$$

and

$$\mu_{\rm in} \approx \frac{B_0^2}{8\pi P_0}. \tag{38}$$

By determining these coefficients self-consistently, the asymptotic relations provide the necessary inner boundary conditions for numerical integration of the ODE system outward, and encapsulate the physical effects of viscosity, magnetic diffusivity, conduction, and advection of the accretion flow.

3.2 Numerical results

The system of nonlinear, coupled ODEs given by equations (22)-(26) is solved numerically to determine the radial structure of the time-dependent, magnetized ADAF in the presence of thermal conduction. The inner asymptotic solutions, given by equations (27)-(31) and the algebraic relations (32)-(38), provide the crucial boundary conditions at a small value of the similarity variable, $\xi_{\rm in}$. We integrate the ODEs outward from this point using a numerical scheme combining a fourth-order Runge-Kutta (RK4) method with an adaptive Fehlberg stepsize control, ensuring accuracy and stability across the vast dynamic range of the solution. Example radial profiles resulting from this numerical integration are shown in Figures 1–3.

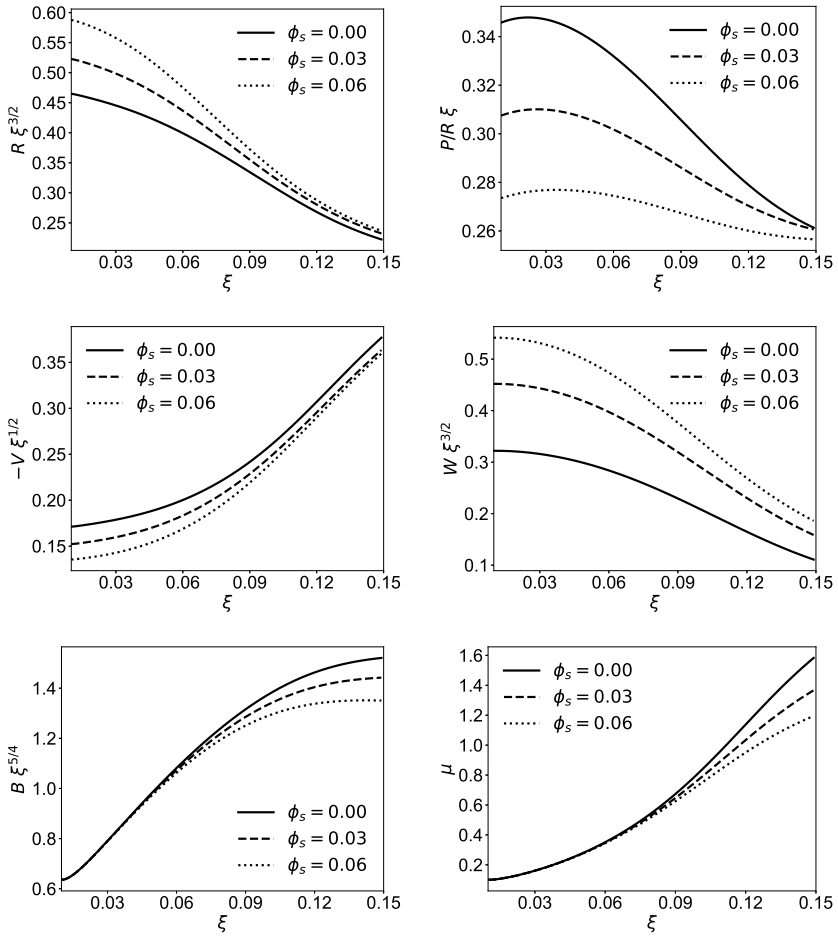

Figure 1: Radial profiles of scaled variables for $\dot{m}_{\rm in} = 1$, $\mu_{\rm in} = 0.1$, $\alpha = 0.3$, $n = 0$, $\eta_0 = 0.6$, $\gamma = 1.5$, $f = 1$ with varying saturated conduction parameter $\phi_s = 0, 0.03, 0.06$. Panels show from top-left to bottom-right: scaled density $R\,\xi^{3/2}$, sound speed $(P/R)\xi$, radial velocity $V\,\xi^{1/2}$, angular velocity $W\,\xi^{3/2}$, toroidal magnetic field $B\,\xi^{5/4}$, and magnetization μ.

To clear the behavior of the flow and facilitate a direct comparison with the canonical steady-state self-similar solutions [10], we plot the scaled dimensionless variables, i.e. $R\xi^{3/2}$, $(P/R)\xi$, $V\xi^{1/2}$, $W\xi^{3/2}$, and $B\xi^{5/4}$. In a steady, self-similar model of a hot flow without additional physics, these quantities are constants independent of ξ. Their pronounced variation with ξ in our solutions is a definitive signature of the flow's essential time-dependence and the complex interplay between accretion, magnetic fields, turbulence, and energy transport. Given that $c_s^2 = p_g/\rho \propto (P/R)t^{-2/3}$ and $r \propto \xi t^{2/3}$, we find $(P/R)\xi \propto (c_s t^{1/3})^2/r$. This scaling effectively normalizes the sound speed by a combination of the temporal and spatial scales.

Figure 1 presents radial profiles of key dimensionless variables for a magnetized, advection-dominated accretion flow, illustrating the influence of the thermal conduction parameter ϕ_s for values 0, 0.03, and 0.06. The significant variation of quantities such as $R\xi^{3/2}$, $V\xi^{1/2}$, $B\xi^{5/4}$, and etc with the similarity variable ξ highlights a solution that is distinctly different

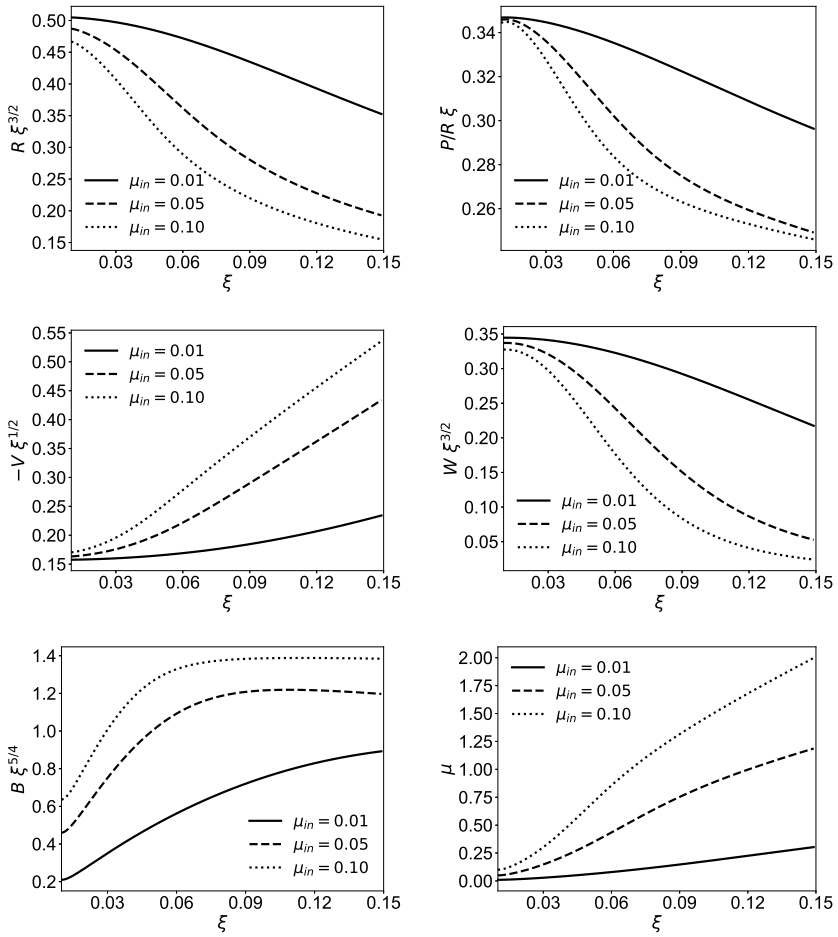

Figure 2: Radial profiles for $\dot{m}_{\rm in} = 1$, $\phi_s = 0.001$, $\alpha = 0.3$, $n = 0$, $\eta_0 = 0.2$, $\gamma = 1.5$, $f = 1$ with several values for magnetization $\mu_{\rm in} = 0.01, 0.05, 0.1$. Panels as in Figure 1.

from steady-state behavior, indicating a time-dependent flow structure. The scaled sound speed $(P/R)\xi$, representing temperature, decreases with increasing ϕ_s, consistent with heat transport via conduction reducing the local temperature. This temperature reduction leads to a decrease in gas pressure and a corresponding increase in gas density within the accreting flow. Furthermore, turbulent viscosity, which is proportional to temperature, weakens with increasing ϕ_s, resulting in reduced viscous torque, an increase in rotational velocity, and a decrease in radial velocity, as confirmed by the profiles. Notably, the ratio of magnetic pressure to gas pressure increases with radius, a feature observed across different parameter values. Finally, the inclusion of thermal conduction leads to a reduction in both the magnetic field strength and the magnetization parameter, likely due to energy transport through conduction affecting the magnetic field configuration and the efficiency of magnetic diffusion.

Figure 2 presents radial profiles of key physical quantities for magnetized accretion flows, illustrating the influence of the magnetization parameter $\mu_{\rm in}$, with $\mu_{\rm in} = 0.01, 0.05, 0.1$, on the flow structure. As $\mu_{\rm in}$ increases, the magnetic field strength and the ratio of magnetic

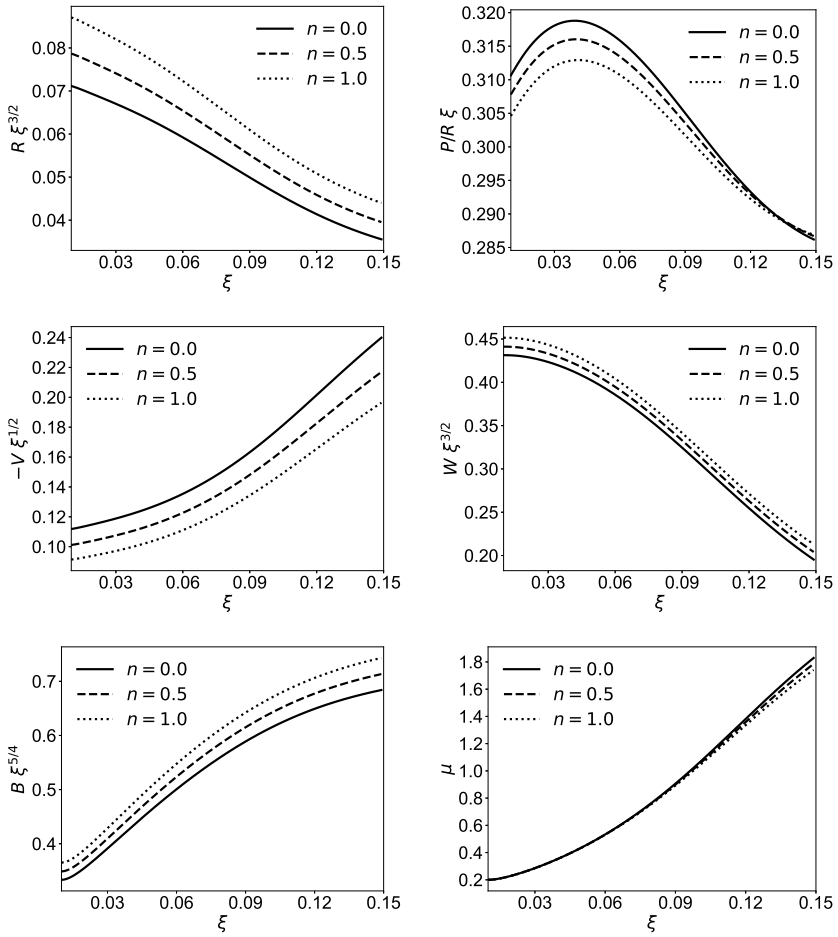

Figure 3: Radial profiles for $\dot{m}_{\rm in} = 1$, $\mu_{\rm in} = 0.2$, $\alpha = 0.2$, $\eta_0 = 0.5$, $\gamma = 1.5$, $f = 1$ with varying turbulence parameter $n = 0, 0.5, 1$. Panels as in Figure 1.

to gas pressure rise, confirming the dominance of magnetic forces. This enhanced magnetic support leads to a decrease in gas pressure and a corresponding reduction in density, with the density profile becoming steeper. This implies a reduction in the radial thickness of the accretion flow, a feature consistent with earlier studies (e.g. [13]). The sound speed decreases with increasing $\mu_{\rm in}$, reflecting the growing contribution of magnetic pressure relative to gas pressure. The radial infall velocity increases with $\mu_{\rm in}$, a behavior qualitatively consistent with Akizuki & Fukue (2006) [14], likely due to magnetic tension forces dominating over magnetic pressure in the radial momentum equation, thereby driving material inward. Conversely, the rotational velocity decreases with increasing magnetic field strength, which can be attributed to the magnetic pressure term in the kinematic viscosity coefficient (equation (5)).

Figure 3 illustrates the radial structure of the accretion flow as a function of the turbulence prescription parameter n, where n governs the pressure support mechanism for the turbulent viscosity and magnetic diffusivity (equations (5) and (6)). Specifically, $n = 0$ corresponds to turbulence fully supported by the total pressure, while $n = 1$ corresponds

to support solely by gas pressure. The observed profiles indicate that increasing n leads to weaker turbulence and reduced turbulent dissipation, evidenced by a decrease in the magnitude of the radial velocity and a corresponding increase in rotational velocity. The temperature profile follows this trend, decreasing as n increases, which is reflected in the sound speed profile. Consequently, the decreasing temperature results in lower gas pressure, causing the density profile to increase across all radii for larger n. Regarding the magnetic field, increasing n leads to an increase in the magnetic field strength. However, the ratio of magnetic pressure to gas pressure exhibits a slight decrease. This latter observation suggests that while the magnetic field itself grows stronger due to the modified transport mechanisms, the accompanying increase in gas pressure (due to weaker turbulence/dissipation) is proportionally larger, slightly diluting the magnetization ratio within the flow structure.

4 Summary and Discussion

This paper presents a time-dependent, self-similar model for magnetized, advection dominated accretion flows that incorporates resistive effects and saturated thermal conduction. Building on the steady-state framework of [10], we derive a set of coupled partial differential equations that describe the evolving radial structure of the flow under the influence of turbulent viscosity, magnetic diffusivity, and non-local energy transport via conduction. Our model accounts for key physical processes such as angular momentum transport via turbulent viscosity and magnetic tension, magnetic field evolution through resistive diffusion, and energy balance involving viscous and resistive heating, and saturated thermal conduction. The inclusion of time dependence allows us to study the transient dynamics of accretion flows, offering a more realistic and dynamic picture than previous steady-state models.

The self-similar formalism enables a reduction of the full partial differential equations to a set of ODEs, which can be solved numerically to obtain radial profiles of density, pressure, velocity, angular velocity, and magnetic field. The asymptotic analysis near the central object reveals power-law behavior, with the structure governed by a balance between gravitational, magnetic, and turbulent forces, as well as energy transport mechanisms. Key physical variables exhibit consistent behavior with recent studies. For instance, our results show that increasing the saturated conduction parameter reduces the sound speed and temperature of the flow, consistent with the findings of Mitra et al. (2023) [15], who showed that stronger conduction transports thermal energy outward and alters the global structure of hot accretion flows. In the model, this leads to a decrease in radial velocity and an increase in the density profile.

The solution in this paper represents that the magnetization parameter increases with radius, a property that can not be seen in steady state self-similar solution (e.g. [14]). The solution in this paper demonstrated that a stronger magnetic field in the accreting flow leads to a reduction in density, and an increase in radial infall velocity. These results highlight the dominant role of magnetic forces in shaping the flow structure. Our model shows that thermal conduction modifies the magnetic field structure and reduces the overall magnetization, likely due to redistribution of thermal energy affecting the field configuration. This behavior is consistent with previous studies, which demonstrate that conduction interacts with instabilities such as the magnetothermal instability and can influence magnetic field in hot accretion flows [16].

In the present model, the accretion flow is analyzed using a one-dimensional approach, neglecting latitudinal variations in physical quantities. A latitudinal study of the model can be explored in future work. We employ a saturated thermal conduction flux. However, some studies use unsaturated conduction and also achieve good agreement with observations (e.g.

[17]). Thus, extending the present model to the unsaturated case would be of interest.

Authors' Contributions

All authors have the same contribution.

Data Availability

No data available.

Conflicts of Interest

The authors declare that there is no conflict of interest.

Ethical Considerations

The authors have diligently addressed ethical concerns, such as informed consent, plagiarism, data fabrication, misconduct, falsification, double publication, redundancy, submission, and other related matters.

Funding

This research did not receive any grant from funding agencies in the public, commercial, or nonprofit sectors.

References

[1] Narayan, R., & Yi, I. 1994, ApJL, 428, L13.

[2] Narayan, R., & Yi, I. 1995, ApJ, 452, 710.

[3] Cowie, L. L., & McKee, C. F. 1977, ApJ, 211, 135.

[4] Tanaka, T., & Menou, K. 2006, ApJ, 649, 345.

[5] Bu, D.-F., Yuan, F., Gan, Z.-M., & Yang, X.-H. 2016, MNRAS, 459, 746.

[6] Balbus, S. A., & Hawley, J. F. 1991, ApJ, 376, 214.

[7] Blandford, R. D., & Payne, D. G. 1982, MNRAS, 199, 883.

[8] Sadowski, A., Narayan, R., McKinney, J. C., & Tchekhovskoy, A. 2015, MNRAS, 447, 49.

[9] Faghei, K. 2012, JAA, 33, 9.

[10] Faghei, K. 2012, Ap&SS, 338, 301.

[11] Ghoreyshi, S. M., & Khesali, A. 2023, PASJ, 75, 52.

[12] Devi, L., Boruah, A. J., & Sarkar, B. 2024, arXiv:2409.11708,

[13] Khesali, A., & Faghei, K. 2008, MNRAS, 387, 145.

[14] Akizuki, C., & Fukue, J. 2006, PASJ, 58, 1033.

[15] Mitra, S., et al. 2023, MNRAS, 523, 4431.

[16] Bu, D.-F., Yuan, F., & Stone, J. M. 2011, MNRAS, 413, 2808.

[17] Shcherbakov, R. V., & Baganoff, F. K. 2010, ApJ, 716, 504.